



**ISSN:2229-6107**



**INTERNATIONAL JOURNAL OF  
PURE AND APPLIED SCIENCE & TECHNOLOGY**

**E-mail :**  
**editor.ijpast@gmail.com**  
**editor@ijpast.in**

**www.ijpast.in**

## Deep Neural Network for Multiple Classification of Brain Tumour Images

P SRINIVASULU<sup>1</sup>, G SUMAN<sup>2</sup>

### ABSTRACT

*Classifying brain tumours is important because it helps doctors assess the lesions and choose the best course of therapy. Imaging can be done in a variety of ways to look for brain lesions. However, MRI is widely used because it produces high-quality images and uses no harmful radiation. As a branch of machine learning, deep learning (DL) has lately demonstrated impressive effectiveness, particularly in the areas of classification and segmentation. In this article, we use two freely accessible datasets to suggest a deep learning (DL) model built on a convolutional neural network for the classification of brain tumours. The former divides malignant growths into (meningioma, glioma, and pituitary tumour). The other one classifies gliomas into three distinct stages (Grade II, Grade III, and Grade IV). The first dataset has 3064 T1-weighted contrast-enhanced pictures from 233 patients, while the second dataset has 516 images from 73 patients. The suggested network topology outperforms the state-of-the-art methods in both experiments, with an average accuracy of 96.13% and 98.7%, respectively. The outcomes show that the algorithm can be used to classify various types of brain tumours.*

### INTRODUCTION

cerebral development is the epitome of the unnatural and the out-of-control.growth in volume of brain cells. Because of the human skull's rigidity and as a result of physical limitations, it's impossible to possible to impact human performance via organ/tissue specificity.and it can spread to other parts of the body from the brain.for the purpose of swaying human behaviour [1]. According to the World Cancer Survey,The newest information from the WHO (WHO),Only 2% of individuals are actually identified with a brain tumour.whenever a very high probability of death or very severe repercussions exists [2].Supporting Organization for Studies on Cancer in the UK, Male It is approximately 5,250 deaths annually are attributed to brain, spinal fluid, and brain stem instances of cancer in the UK [3].For instance, there are several methods to classify brain lesions.tumours that are not the primary or secondary type. Roughly a third of all.Approximately 70% of brain cancers are considered to be tertiary.With a 30% surplus rate. This categorization is intended for use with,Like most malignancies, tumours have a neurological origin.tumours in the major blood vessels. On the other hand, cancers start in signal sent to the brain from other parts of the body are

A

alignant secondary development.malignant secondary development sadly dominates the statistics [4].The associate editor who will be in charge of seeing that this work gets reviewed and The ultimate publication was approved by Yutong Zhang.Multiple testing approaches can be used to Us need a system for classifying brain tumours. However, magnetic resonance imaging (MRI) is among the most widely used diagnostic procedures.common practices that don't require damaging the material being worked on. How the fad for MRIs got started Scanning did not involve the use of any potentially dangerous radioactivity.in addition to it's excellent transparency in soft tissues and its ability to mass a series of shots taken at different exposures or through the incorporation of contrast-enhancing chemicals, as detailed in [5] and [6].Gliomas, the most prevalent type of brain malignancy, originate in glial cells of the brain [7]. Glioma Types and Illustrations The Central Nervous System (CNS) is thought to be the site of origin for up to 30% of all

---

**Assistant professor<sup>1,2</sup>**

DEPARTMENT OF ELECTRONICS AND COMMUNICATION ENGINEERING

P.B.R. VISVODAYA INSTITUTE OF TECHNOLOGY & SCIENCE S.P.S. R NELLORE DIST, A.P, INDIA, KAVALI-524201

---

tumours. Meningiomas in the skull [7]. Gliomas are divided into four groups using WHO classifications (types I through IV) [8]. Grade I appearance and texture, benign type I masses are most similar to Grade II glial cells are very similar in composition to regular glial cells. Grade III malignant tumours exhibit atypical features. Grades I through IV, the most severe being glioblastomas, and abnormalities in cellular shape that can be seen [1]. Cancerous development on the membrane that surrounds the brain is called a meningioma. It includes the area inside the skull that contains the central nerve system and grows without violence. Most tumours caused by meningioma are benign [8]. Pituitary cancers, on the other hand, begin in the pituitary glands themselves. Substances that regulate physiological functions. It is feasible, in fact, moderate, moderate with bone tumours, and serious. Com-Hormone output can be affected by a pituitary tumour for a very long time.

**disability or loss of vision [1].**

Given the foregoing information, early identification.

The diagnosis and classification of brain tumours are now critical responsibilities.

analysis of the situation and advice on how to improve simple treatment that has helped save a lot of lives [8]. Further- Furthermore, classifying things can be a laborious and time-consuming procedure. Complicated medical circumstances present a greater task for physicians and specialists to resolve. In these cases, diagnosis, localization, and treatment all necessitate the assistance of specialists. Tumour cells are filtered and compared to their surroundings. So That Viewers Can Understand Them Better sense and arrive at a conclusive verdict; in the instance of a development, whether it is if we know how to categorize it. Although this task can be tedious, computer-aided design (CAD) software can save a lot of time and effort. With the aid of a computerized system, brain tumours can be discovered at an early stage. decreasing pace at

which humans must intervene. The study of computational models, including programs and data structures (ML statistical procedures for achieving a specified goal undertaking with no clear instructions and a reliance on tried and tested terns are used instead [9]. Machine learning algorithms have emerged as an AI subsystem in the medical imaging industry cunning [6]. It can be broken down into two broad categories: separated into regulated and wild groups. Under close guidance, when using technology, procedures, there are several methods for calculating a translation function. variables and the titles of the outcomes we expect them to produce Modified the subject titles. Independent study is the primary computer-aided pattern identification in the instruction materials in the same vein as an SVM or Neural Network [10] or K-nearest neighbours (KNN) [11]; alternatively, a support vector machine. While the output of guided learning is considered, it is not the input, combined with the idea of self-organization and imprecise c-means [12], SOM, or the System Object Model, [13]. Characteristics must be derived from the majority of educational illustrations are grayscale, smooth, and unmoving. Learning-enhancing statistical features that may It is common practice for tumour division to precede feature extraction. stage. Because of the time and care put into their creation, we call these elements "handcrafted." one who has mastered their subject through years of practice and study figure out which ones are the most crucial. Moreover, this Managing task of this nature is time-consuming and error prone. Data collection on a grand stage [14]. Deep Learning (DL) is a subset of machine learning (ML) that relies heavily on Learning how to describe data and how to organize features into hierarchies The tiered structure that deep learning algorithms depend on attributes for feature retrieval using nonlinear processing. The A layer's output becomes part of the input for the following layer. As we learn more specifics, this helps with overarching conclusions.

connection [15]. Among the many varieties of artificial neural networks is the CNN, or

convolutional neural network. common DL application in the field of image analysis and built in such a way that minimal preliminary labour is required [16]. It is impacted by studies of the human brain [17] employed in the handling of data supplied in a wide range of matrix forms [18]. The first-of-its-kind use of a deep convolutional neural network to solve it's no secret that there's been a revival of the In the latter part of the 20th century, Lacuna was the first to introduce the idea of a deep neural network. It is a tool used by text recognition software. In 1998 [19]. After a lengthy wait, it finally started to gain traction, regular right after using a deep convolutional neural network making use of (ImageNet LSVRC-2010) a collection for classifying images. As a method, (Alex Net) [20] is being used. Alex Net is remarkable because of

#### contrasts with other prevalent network designs

period of life. As a result of its success, a spinoff series was created. Success stories in deep learning where CNNs played a role. The main advantages of CNNs are in their ability to acquire new features and Unlike regular machines, it can produce results with a high degree of precision. both learning and simple neural networks are within reach. when there is more information to learn from, performance increases. [6] A reliable and accurate model. The conventional CNN layout has the convolutional filters, which are also used as feature extractors, are currently in use. The further we delve, the more complex features we strip away. (Specific spatial and conceptual information). Disentanglement of Individual Features styluses by splicing together the results of multiple small filters next, identifying the most salient features, and Launching the training of the categorization network is the next stage [18]. Brain tumours have been categorized in a variety of ways. Using Imaging Resources and Algorithms for Machine Learning Ages go by. In 2009, Zacharaki et al. [21] proposed an approach. In order to further classify gliomas beyond a yes/no framework, grade separation using support vector machines and kernel neural networks. The overall precision of the categorization is 88%, with 85% being reached in the multi-classified. in terms of a binary option. El-Dashan et al. [22] first introduced Analysis of 80 brain tumours, dividing them into normal and abnormal subtypes. Digital image data mining (DWT) is one such technique. features, distilling the information with Patriates, then ANN, and finally KNN, for image labelling.

100% dependability for both 98% and 99%. In 2015,

Cheng et al. [23] proposed a method for enhancing cognitive abilities.

enhance tumour grading precision by fortifying tumour region by first zooming out and then breaking the image down into more manageable regions. The experts used three techniques to pick out distinguishing characteristics: density matrix of grayscale occurrences and co-occurrence matrix (GLCM) used in tandem with the BOW for maximum precision with a combined accuracy rate of 91.28 percent using ring-shaped tumour segmentation and

#### lengthening a specified region.

In their article, Ertegun and Rubin [24] propose a solution. The authors used CNN to classify various kinds of gliomas. diagnostic images (Grades II, III, and IV), and another task classifying gliomas as either High-Grade (HG) or Low-Grade (LGG) (LGG). Grading Gliomas (HGG). There was an improvement in accuracy to at least 71%. There is a correlation of 96% between the two. Paul et al. [25] used a sagittal brain tumour as their model. illustrations for studying and exercising the two most fundamental kinds of categorization to classify data (using a convolutional neural network that has a full architecture of a convolutional neural network (or simply a convnet) is the outcome of fusing two layers, two max-pooling layers, and a number of convolutional layers. first two layers that are fully interconnected, and then a third stratum that to within 91.43% of the true value at most. Regarding the conclusion, Afshar et al. [26] showed a container network (Caps Net) that integrates classification via magnetic resonance imaging (MRI) of the brain and protruding tissue. The development in the brain solidified. We have a 90.89 percent success rate. While conducting this inquiry. Similar procedures were proposed by Anarkali et al. [27] in their study. Using only two rules, we develop a classification algorithm for brain tumours. neural network and a graphical representation of a genetic algorithm (GA-CNN), The accuracy was 90.9% on the first test case.

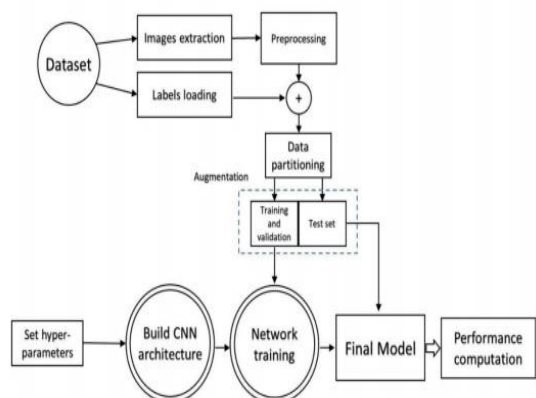


**FIGURE 1. Block diagram of the proposed method.**

while 94.2% precision was achieved in dividing gliomas into three categories, use in glioblastoma, meningioma, and pituitary tumour categorization in the second case study, these conditions are met. In this article, we suggest a convolutional neural network (CNN) design for classification purposes. Various forms and stages of malignant brain tumours. Design structure of the network is developed by trying out new setups in order to get the best framework for your needs. An outline has been provided for this presentation as follows; the suggested approach is described in Section 2. discussed in depth, beginning with the initial data collection and moving on to how adjustments are made to the CNN algorithm so that it works with the resources and equipment employed in this study. Chapters 3 and 4 are devoted to the findings and the debate, accordingly, and then Part 5 provides a wrap-up.

## METHOD

The blocks of the suggested procedure are depicted in FIGURE 1. wherein the system initiates picture loading and extraction and names from the raw files of datasets and then perform some sort of cleaning and enhancement methods immediately following dataset partitioning divided into groups for instruction, testing, and evaluation. After that, the framework of After establishing the need for the suggested technique, it is presented. optimization, regularization methods, and hyper-linked algorithm. Lastly, we will discuss network efficiency and training. Mathematical results are displayed.

## DATASET

In this study, we employ two data sets. Here's the first gathered from the General Hospital and Nanyang Hospital Between 2005 and 2010 [23], at China's Tianjin Medical Institute. after which it was

released online in a number of different forms 2015, with the final instalment coming out in 2017. Data source pictures taken with T1-weighting and contrast enhancement meningioma, glioblastoma, and pituitary tumour, originating from 233 individuals [28]. Brain Tumours can vary in size, position, and appearance depending on several factors. according to their classifications in FIGURE 2 (a). Axial, sagittal, and oblique perspectives are all represented in the collection. Figure 2 shows the axial and transverse perspectives (b). The secondary The Cancer Imaging Collection provides the information (TCIA) source open to the world [29]. The Central Database of Molecular data on large brain tumours (REMBRANDT).

sequences of pictures from 130 individuals suffering from a wide range of ages, genders, racial/ethnic identities, and academic levels [30]. Images were chosen from T1-weighted improved contrast images of varying grading levels (Grades II, III, and IV) of glioblastoma Fig. 3. Additional information is provided in Tables 1 and 2. regarding the relative descriptions of the two databases

## STAGE PRIOR TO PROCESSING

To ensure that the suggested framework is capable of handling the input pictures, a pre-operation is carried out. The initial step is a down-compress the original 512x512 picture into 128x128 pixels to reduce dimensions, compressing computations and aid the network in functioning more effectively. requiring less effort and time and leading to simpler computations. Then, In order to keep the system running smoothly, data is jumbled before being divided. training on uncategorized data to avoid overspecializing a particular data set's band size. The information is presented in three parts; Each of the three sets—training, certification, and testing—has its own unique categories to aim for (68% in instruction, 32% in testing, and validation). At last, we enhance the pictures used in scientific research that they are distinguishable as fresh by the system, and commonly employed to prevent model overfitting and boost robustness [20], [31]. Furthermore, this linear improvement The pictures are distorted by adding a monochrome noise effect (sodium noise).

*PICTURE 4 compares the enhanced examples given here with the*

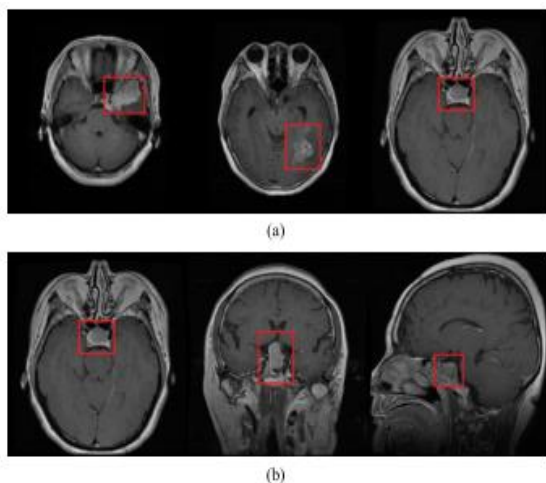


**FIGURE 2.** (a) Different three axial brain tumour types as follows; in this series of images, we first see (a) a meningioma, then (b) a glioma, and finally (d) three different obtained views of the pituitary tumour, in the axial, coronal, and sagittal planes. The Sarcomas are.

within the confines of the crimson square's boundaries.

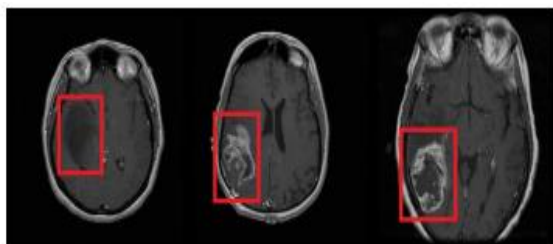


**FIGURE 3.** Different glioma grades included in REMBRANDT dataset (Grade II, Grade III and Grade IV from left to right respectively). Tumours are localized inside.

a red rectangle.

**TABLE 1.** Number of slices for each brain tumour type (meningioma, glioma and pituitary) in dataset I and their corresponding number of patients.

| Tumor Category | Number of Patients | Number of Slices |
|----------------|--------------------|------------------|
| Meningioma     | 82                 | 708              |
| Glioma         | 91                 | 1426             |
| Pituitary      | 60                 | 930              |
|                | 233                | 3064             |

original one; for study I, we flipped it on its x-axis, mirrored it right to left, added salt noise, and rotated the picture by 45 degrees. Using this method of enhancement, our finished collection included 15,320 pictures for Study I and 516 images for Study II, an increase of a factor of 5 from the initial 3064 images.

## PROPOSED CNN ARCHITECTURE

The suggested CNN architecture is depicted in FIGURE 5. The first of its 16 levels store the enhanced pictures from the previous pre-processing phase, the input layer.using activation functions of convolution layers

**TABLE 2.** Number of slices for glioma grades in dataset II and their corresponding number of patients.

| Tumor Category | Number of Patients | Number of Slices |
|----------------|--------------------|------------------|
| Grade II       | 33                 | 205              |
| Grade III      | 19                 | 129              |
| Grade IV       | 21                 | 182              |
|                | 73                 | 516              |

the layers used for convolving, Rectified Linear Unit (REL) normalizing, pooling, and selecting features. A dropout layer is used to avoid overfitting.

and then a completely linked layer, a SoftMax layer for output prediction, and finally a classification layer for generating the expected class. Here's how we break down each layer: To begin, we use the input layer to verify the input pictures' sizes and implement a data standardization [20]. The suggested design features three convolutional layers. Sliding K convolutional filters (kernels) of size (M N) are applied to the input pictures in a 2D convolutional layer, and the dot product of the weights (kernels) is calculated.

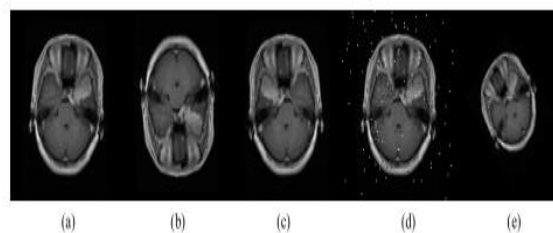


**FIGURE 4.** (a) The original image, (b) up-down flipping, (c) right/left mirroring, (d) add

salt noise to the image, (e) rotating by 45 degree.

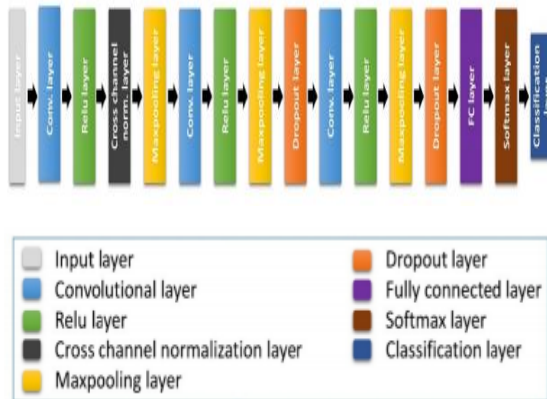


FIGURE 5. The proposed CNN architecture.

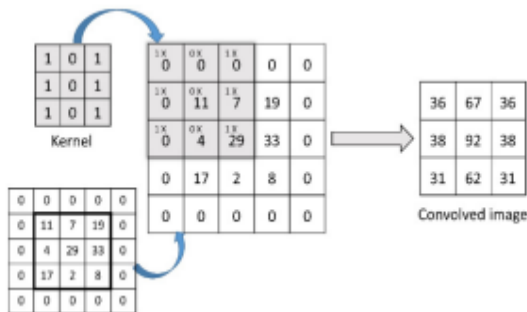


FIGURE 6. Convolutional layer example (input: 3x3, zero padding: 1, kernel size: 3x3, Stride: 1, output: 3x3).

input, and weights) and input. Stride is the vertical and horizontal strides the filters take as they move across the picture (S). The initial pictures may be padded with zeros (P) before the filters are dragged over them. In order to keep data at the periphery. These kernels are used as feature identifiers, with lower-level features (edges, lines, and clumps) being detected by kernels in the first few levels and higher-level features being detected by kernels in the later layers [19]. FIGURE 6 depicts an illustration of putting a kernel of size 3 3 (appearing in dark) over a picture of size 3 3, resulting in input measurements of 3 3.  $K = 64, 128, \text{ and } 128, M \times N = 10 \times 10, 3 \times 3, \text{ and } 2 \times 2, S = [1, 1], P = [0,0,0,0], [2,2,2,2], \text{ and } [2,2,2,2]$  for the convolutional layer, and  $[0,0,0,0], [2,2,2,2], \text{ and } [2,2,2,2]$  for the pooling layer.

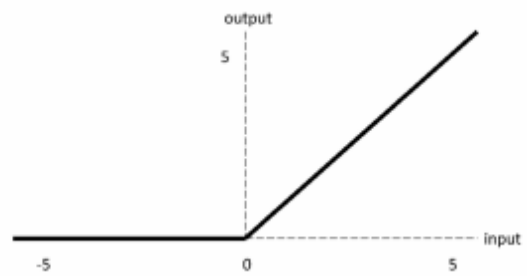


FIGURE 7. REL activation function.

In order, they are levels 1, 2, and 3. In order to drastically cut down on training time, a non-saturated activation function called REL is used as the layer that follows every convolutional layer. When put next to various other activation functions [20, 32, 33]. The REL model can be expressed as a function of  $x$  with the following expression, where the result matches the input when  $x$  is positive and 0 otherwise [33]. FIGURE 7: A pictorial representation of the REL function, where  $f(x) = \max(0, x)$ . The input layer is then normalized by scaling and modifying the active-tons in a cross-channel normalization layer. It creates a layer of adjustment for the local answer using a channel-wise frame of a fixed size (here, 5). The standardization is helpful for accelerating backpropagation and network training [20, 32].

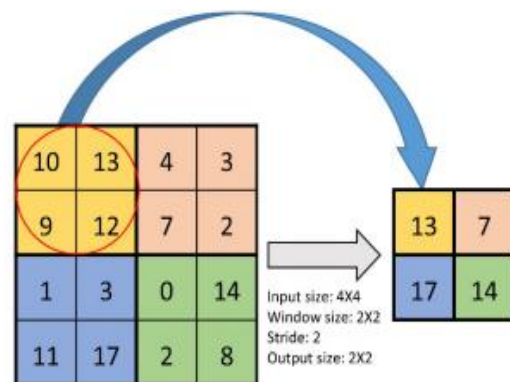


FIGURE 8. Example of a max-pooling layer (the maximum value out of a

viewport (only those of the same hue are taken into account). Maximum Pooling layer, on the other hand, is a down-Spatial invariance can be attained through sampling by randomly portion of the picture into squares (2 by 2 in the suggested shape) that are scooting over the picture with a purposeful stage (2 2) and then focusing on the highest possible result. The four fundamental ingredients. Pooling layer is employed for lowering factors and, by extension, calculations in the linkage

[34, 35]. The max-pooling layer is illustrated by illustrated by FIGURE 8. In order to lessen the likelihood of overfitting, exit layering (an example is shown in FIGURE 9). This layer is responsible for removing unnecessary activations (nodes) randomly, which also aids immensely in boosting the train's speed-to the Ing step [36]. We discovered that in the suggested architecture The most optimal loss rates were 10% and 20%. dropout layer 1 and dropout layer 2 numbers. Then, we used three cutting-edge elements, including Completely Con-classification layer, the SoftMax layer, and the connected layer (FC). The earlier one is used to link all a layer's neurons together cell in a different one; the resultant output Three types constitute this stratum. Once the FC stratum has been reached by a (normalized exponential) SoftMax layer. function). All the forecasted data is compressed using a SoftMax layernumbers between 0 and 1, the grand total of which is ratio of 1 (100%) to another value. It is possible to compute this layer's.

**result.in this way:**

It is possible to determine the likelihood of any group (j) by using (k)the aggregate of squares for all classes plotted against y (z).proportions are 1, as depicted in FIGURE 10. Finally,we use a cross-entropy based classification layer.loss to calculate an approximation of the classification expected class title for each of the supplied pictures. Damage cantarget identifiers p can be determined using equation (3).vector, and q (x) represents the SoftMax layer's final output vector.

$$H(p, q) = - \sum_x (p(x) * \log(q(x))) \quad (3)$$

**REGULARIZATION TECHNIQUES AND OPTIMIZATION ALGORITHM**

By avoiding system overfitting during training, regularization allows for a good match of a solution function during training. Overfitting has been avoided in preproduction through a variety of methods.

stages of stopping and training. To begin, overfitting can be prevented through the use of data enhancement by applying a geometry and colour distortion to the source pictures [23], [31], [38]. Then, various network designs have been tried out to see if they can reduce network complexity. The weights of hidden units can then be removed in a random fashion using dropout layers [36], [39]. The following equation [40] illustrates how L2

regularization is used to penalize the cost function and introduce weights decline.

$$Cost\ function' = Cost\ function\ (Loss) + \lambda \sum_{i=1}^k w_i^2 \quad (4)$$

where is the regularization parameter (specified hyper-parameter), and w is the weight(s) associated with iteration I from 1 to last but not least, the "early halt method" has been implemented in a few tri-training is terminated prior to the end of a period if the system is stable or if overfitting is detected by an auxiliary learning system (also) [40].

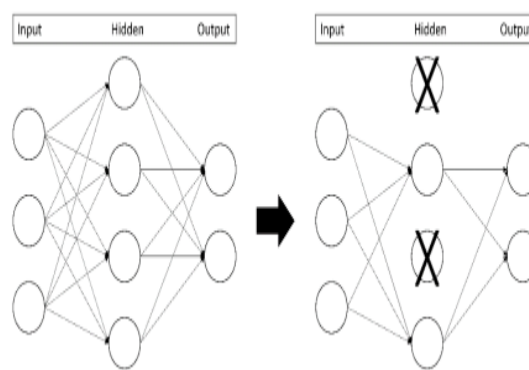


**FIGURE 9. Example of dropout layer (probability of 50% appears on the right).**

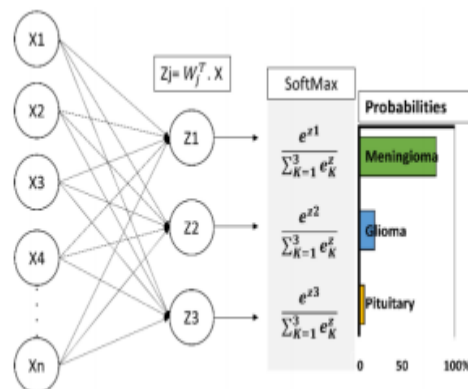


**FIGURE 10. Example of Soft-max layer.**

Optimizing a network typically entails making minor, incremental changes to the negative gradient until the loss function is at its world minimum.net (convergent) path [41]. For the suggested architecture, we discovered that the "stochastic gradient descent with momentum" is the best algorithm.

**EXPERIMENTS AND RESULTS**

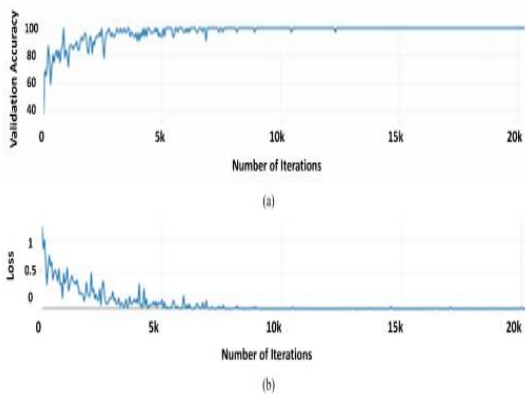


In PICTURE 11, we can see the gains and losses in precision that our suggested network experienced during the evaluation portion of study I. EXHIBIT 11(a) demonstrates that nearly one hundred percent precision

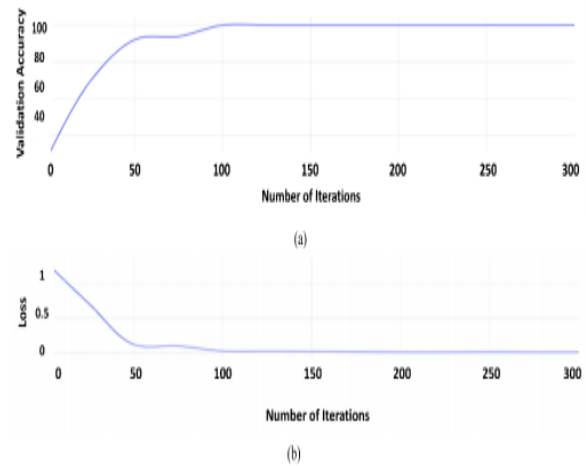
success after only 5000 trials. The accuracy reaches a peak at nearly 100% after 8550 iterations, and the highest total accuracy achieved in the testing period is 96.13 percent. Figure 11(b) is a loss graph for mini-batches, and it's easy to see how the slope drops abruptly at first before showing some fluctuations because of the tiny mini-batch size. After 6400 rounds, these variations typically vanish and the loss trajectory nearly reaches zero.

EXHIBIT 12 displays the gains and losses in precision experienced by study II during the confirmation stage. As shown in FIGURE 12(a), full precision was reached after only 100 trials. Therefore, the highest level of test-phase precision achieved was 98.7%. As can be seen in FIGURE 12(b), a steep decline can be observed in the mini-batches loss histogram.

After the century mark, this incline typically disappears.



**FIGURE 11.** Validation accuracy and loss over the whole training iterations of study I: (a) Validation accuracy (higher is better), and (b) Loss (lower is better).



**FIGURE 12.** Validation accuracy and loss over the whole training iterations of study II: (a) Validation accuracy (higher is better), and (b) Loss (lower is better).

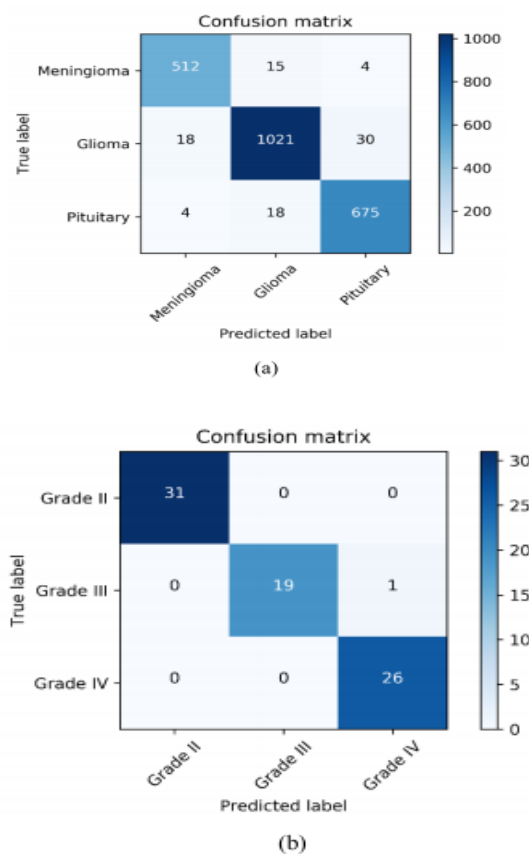


**FIGURE 13.** The confusion matrix of the proposed model: (a) for study I, and (b) for study II. TABLE 3. Accuracy metrics in terms of TP, TN, FP, FN, precision, sensitivity, specificity, and accuracy.

| Method                      | Metrics<br>Tumor Type | TP   | TN   | FP | FN | Precision    | Sensitivity  | Specificity  | Accuracy      | Total no. |
|-----------------------------|-----------------------|------|------|----|----|--------------|--------------|--------------|---------------|-----------|
| Proposed Model for Study I  | Meningioma            | 512  | 1744 | 22 | 24 | 0.958        | <b>0.955</b> | <b>0.987</b> | <b>97.54%</b> | 547       |
|                             | Glioma                | 1021 | 1195 | 33 | 61 | <b>0.972</b> | 0.944        | 0.951        | 95.81%        | 1069      |
|                             | Pituitary             | 675  | 1566 | 34 | 48 | 0.952        | 0.934        | 0.97         | 96.89%        | 697       |
| Proposed Model for Study II | Grade II              | 31   | 46   | 0  | 0  | 1            | 1            | 1            | <b>100%</b>   | 31        |
|                             | Grade III             | 19   | 57   | 0  | 1  | 1            | 0.95         | 1            | 95%           | 20        |
|                             | Grade IV              | 26   | 50   | 1  | 0  | 0.963        | 1            | 0.98         | <b>100%</b>   | 26        |

### CONFUSION MATRIX

Confusion vectors summarizing system performance across both trials are depicted in FIGURE 13. (I and II). Predicted values (system output) are shown along the X-axis, while actual values The real markings can be seen along the Y-axis (ground truth). Equation 5 was used to determine the values for precision, sensitivity, specificity, and accuracy.

$$\text{Precision} = \frac{TP}{(TP + FP)}$$

$$\text{Sensitivity} = \frac{TP}{(TP + FN)}$$

$$\text{Specificity} = \frac{TN}{(TN + FP)}$$

$$\text{Accuracy} = \frac{(TP + TN)}{(P + N)}$$

were,

The number of occurrences that test positive, or True Positive (TP), is the proportion of accurately predicted positive cases. When someone says "real negative," what exactly do they mean? Circumstances, and they're also not optimistic when you think about it. A (type two) error is the occurrence of a positive result when a negative result was anticipated. Type one error, also called a fake positive, is the occurrence of a result that was predicted to be positive but actually was not (FP). Precision metrics obtained from the uncertainty matrix are shown in Table 3. The highest achievers in terms of precision, sensitivity, specificity, and accuracy are highlighted in Table 3. The success rates for classifying meningioma, glioma, and melanoma are respectively 97.54%, 95.81%, and 96.89%.

**ABLE 4. Different architectures and hyper-parameters tested and tried before reaching the final model.**

| Factor(s)                                    | Values                       |
|--|------------------------------|
| Number of convolutional + ReLU layers        | 1, 2, 3, 4                   |
| Number of cross-channel normalization layers | 1, 2, 3                      |
| Number of drop out layers                    | 1, 2, 3                      |
| Maximum epochs                               | 20,40,50,60,80,100           |
| Number of fully connected layers             | 1, 2, 3                      |
| Number of convolutional kernels              | 8, 16, 32, 64, 128, 256      |
| Kernel size                                  | 2, 3, 5, 7, 9, 10, 11        |
| pooling layer                                | Max pooling, average pooling |
| pooling layer window size                    | 2, 3, 4, 5                   |
| Optimizers                                   | SGD, Adam, RMSprop           |
| Mini-batch size                              | 1, 4, 8, 16, 32, 64, 128     |
| Dropout rate                                 | 0.1, 0.15, 0.2, 0.25, 0.5    |
| Initial learning rate                        | 0.01, 0.001, 0.0001          |
| Learning rate drop factor                    | 0.1, 0.2, 0.3                |

**TABLE 5. Comparison between the proposed model and previous related works.**

| Model                           | Best Accuracy for Study I | Best Accuracy for Study II | Classification Type | Classification Method |
|---------------------------------|---------------------------|----------------------------|---------------------|-----------------------|
| 1 Cheng <i>et al.</i> [23]      | 91.28%                    | -                          | Multi               | SVM and KNN           |
| 2 Paul <i>et al.</i> [25]       | 91.43%                    | -                          | Multi               | CNN                   |
| 3 Alshar <i>et al.</i> [26]     | 90.89%                    | -                          | Multi               | CNN                   |
| 4 Anaraki <i>et al.</i> [27]    | 94.2%                     | 90.9%                      | Multi               | GA-CNN                |
| 5 Zacharaki <i>et al.</i> [21]  | -                         | 85%                        | Multi               | SVM and KNN           |
| 6 Zacharaki <i>et al.</i> [21]  | -                         | 88%                        | Binary              | SVM and KNN           |
| 7 El-Dahshan <i>et al.</i> [22] | -                         | 98%                        | Binary              | ANN and KNN           |
| 8 Ertosun <i>et al.</i> [24]    | -                         | 71%                        | Multi               | CNN                   |
| 9 Ertosun <i>et al.</i> [24]    | -                         | 96%                        | Binary              | CNN                   |
| 10 Proposed structure           | <b>96.13%</b>             | <b>98.7%</b>               | Multi               | CNN                   |

**Pituitary classification. However, we achieved an accuracy of 100% in classifying glioma Grade II, 95% for glioma Grade III and 100% for glioma Grade IV.**

### EMPIRICAL ARCHITECTURES AND HYPER-PARAMETERS

In this section, we detail the many design considerations that go into creating these building choices. Table 4 displays the outcomes of these early experiments. finishing the best-possible framework presentation in terms of performance.

### TOOLS AND TIME CONSUMPTION

MATLAB 2018b, Python, and 16 GB of RAM are used to train the suggested deep neural network structure on the NVIDIA GTX 1060 Processor (with 6 GB of memory). The InstructionThe first

research took 289 minutes and had 10,417 pictures, while the second only took 2.5 minutes and had 350 images. Research I and II had corresponding average test run times of 8.5 and 9.6 milliseconds per picture.

## DISCUSSION

There is a thorough breakdown and classification of brain tumours. A convolutional neural network model is suggested for tumour classification by comparison with X-ray pictures. Many factors influence CNN modelling, are implemented to allow system setup prior to design completion. texture. Attempting to train a Network from start is famously difficult, created in an instant, a week, or a month. Without artificially skewing the results. Consequences of Prior studies employing analogous kinds of brain tourniquet configurations, hyper-settings, and levels presented in Table 5's data. The suggested architecture has some obvious advantages. Provides the most accurate forecasts compared to alternative methods. Previous research has demonstrated the benefits implied structure. As a means of classification, the suggested CNN technique is recommended. Simple method as we illustrate how the brain develops to something that has a solid connection to it. However, feature engineering was used to retrieve in [21-23]. characteristics, and distilled them for use in This is the next level of classification. The writers of [27] have clearly used GA as a metaphor for network structure, but However, GA did not perform better than conventional methods in terms of the accuracy of its predictions. Two convolutional layers are all that are used by the writers in [25]. processors with 64 independent cores. In addition, they have employees There are found to be four levels of notable loss. Network. While this has been done with pathos- logical thinking, Ertegun and Rubin [24] argue that Training networks with jumbled up pictures has been unsuccessful so far. found by fusing the results of two other programs. In [26], The writers have also made use of tumours with hazy borders. data that can aid the network in displaying findings more accurately. The Human intervention is required at the previous, identifying, step. dangerous for a Reporter to work without first receiving instruction. We've Gotten Some Good Out of It, But

**The suggested technique achieves encouraging classification findings.**

These findings need to be verified with larger databases. Recruit from both gender and all walks of life to widen its appeal. And eventually try it out

for other medicinal applications. Not only that, but the framework of the method is not transferable between lessons. Simplifying a limited set of pictures is a common task in deep learning. Ing restrictions, but rather the method can be adjusted to meet the needs of the individual fine-tuned after extensive data training to affect subtle details dataset.

## CONCLUSION

In this paper, we present a computer-aided diagnosis (CAD) method for separating MR pictures of brain tumours into three distinct categories: meningioma, glioma, and pituitary. Using a specialized deep neural network architecture, gliomas are classified into classes (II, III, and IV). The suggested network consists of 16 layers, beginning with an input layer that stores the pre-processed pictures and continuing on through three convolution layers, three REL layers, a normalization layer, and three Carpooling layers to complete the network. In addition, a completely linked layer and a SoftMax layer are used to forecast the output, and a class- fiction layer generates the expected class, with two dropout layers included to avoid overfitting. Data enhancement proved effective in displaying improved findings despite the comparatively small dataset (due to the diversity of imaging perspectives). With the two datasets we used for this study, our suggested design obtained a precision of 96.13% and 98.7%, respectively.

## REFERENCES

- [1] L. M. De Angelis, "Brain tumours," *New England J. Med.*, vol. 344, no. 2, pp. 114–123, Jan. 2001.
- [2] B. W. Stewart and C. P. Wild, *World Cancer Report 2014*. Lyon, France: IARC, 2014.
- [3] *Brain, Other CNS and Intracranial Tumours Statistics*. Accessed: May 2019. [Online]. Available: <https://www.cancerresearchuk.org/>
- [4] A. Behin, K. Hoang-Xuan, A. F. Carpentier, and J.-Y. Delattre, "Pry- Mary brain tumours in adults," *Lancet*, vol. 361, no. 9354, pp. 323–331, 2003.
- [5] A. Defleas, *Imaging of Brain Tumours With Histological Correlations*. Berlin, Germany: Springer, 2002.
- [6] G. Listens, T. Kooi, B. E. Bernarda, A. A. A. Setia, F. Ciampa, M. Ghafoor Ian, J. A. W. M. van der Laak, B. van Ginneken, and C. I. Sánchez, "A survey on deep learning in medical image

analysis,” *Med. Image Anal.*, vol. 42, pp. 60–88, Dec. 2017.

[7] M. L. Goodenberger and R. B. Jenkins, “Genetics of adult glioma,” *Cancer Genet.*, vol. 205, no.12, pp. 613–621, Dec. 2012.69224May

[8] D. N. Louis, A. Perry, G. Reifenberger, A. von Deimling, D. Figarella-Branger, W. K. Cavenee, H. Ohtaki, O. D. Wiestler, P. Kalise, and D. W. Ellison, “The 2016 World Health Organization classification of tumours of the central nervous system: A summary,” *Acta*

*Neuropathology.*, vol. 131, no. 6, pp. 803–820, Jun. 2016.

[9] C. Bishop, *Pattern Recognition and Machine Learning*. Berlin, Germany: Springer-Verlag, 2006.

[10] T. Rajesh and R. S. M. Malar, “Rough set theory and feed forward neural network based brain tumour detection in magnetic resonance images,” in *Proc. Int. Conf. Adv. Nanomaterials Emerg. Eng. Technol. (ICANMEET)*, Jul. 2013, pp. 240–244.

[11] K. Machala, H. B. Anandpur, V. Kapur, and L. Kosta, “MRI brain cancer classification using hybrid classifier (SVM-KNN),” in *Proc. Int. Conf. Ind. In strum. Control (ICIC)*, May 2015, pp. 60–65.

[12] M. Shashidhar, V. S. Raja, and B. V. Kumar, “MRI brain image segmentation using modified fuzzy C-means clustering algorithm,” in *Proc. Int. Conf. Common. Syst. Newt. Technol. (CSNT)*, Jun. 2011, pp. 473–478.

[13] S. Goswami and L. K. P. Bhuiya, “Brain tumour detection using unsupervised learning based neural network,” in *Proc. Int. Conf. Common. Syst. Newt. Technol. (CSNT)*, Apr. 2013, pp. 573–577.

[14] S. Khalid, T. Khalil, and S. Nasreen, “A survey of feature selection and feature extraction techniques in machine learning,” in *Proc. Sci. Inf. Conf.*, Aug. 2014, pp. 372–378.

[15] L. Deng and D. Yu, “Deep learning: Methods and applications,” *Found. Trends Signal Process.*, vol.7, nos. 3–4, pp. 197–387, Jun. 2014.

[16] Y. Lacuna. (2015). *Lenet-5, Convolutional Neural Networks*. Accessed:2019. [Online]. Available: [HTTP://yann.lecun.com/exdb/lenet](http://yann.lecun.com/exdb/lenet)

[17] M. Mitsugi, K. Mori, Y. Mitarai, and Y. Kaneda, “Subject independent facial expression recognition with robust face detection using a convolutional neural network,” *Neural Newt.*, vol. 16, nos. 5–6, pp. 555–559, Jul. 2003.

[18] Y. Lacuna, Y. Bagnio, and G. Hinton, “Deep learning,” *Nature*, vol. 521, no. 7553, p.436, 2015.

[19] Y. Lacuna, L. Bottom, Y. Bagnio, and P. Haffner, “Gradient-based learning applied to document recognition,” *Proc. IEEE*, vol. 86, no. 11, pp. 2278–2324, Nov. 1998.[20] A. Hrushevsky, I. Subsieve, and G. E. Hinton, “ImageNet classification with deep convolutional neural networks,” in *Proc. Adv. Neural Inf. Process. Syst. (NIPS)*, Jan. 2012, pp. 1097–1105.

[21] E. I. Zacharaki, S. Wang, S. Chawla, D. S. You, R. Wolf, E. R. Melhem, and C. Davanzo’s, “Classification of brain tumour type and grade using MRI texture and shape in a machine learning scheme,” *Magn. Reason. Med.*, vol. 62, no. 6, pp. 1609–1618, Dec. 2009.

[22] E. S. A. El-Dashan, T. Hosny, and A. B. M. Salem, “Hybrid intelligent techniques for MRI brain images classification,” *Digit. Signal Process.*, vol. 20, pp. 433–441, Mar. 2010.

[23] J. Cheng, W. Huang, S. Cao, R. Yang, W. Yang, Z. Yun, Z. Wang, and Q. Feng, “Enhanced performance of brain tumour classification via tumour region augmentation and partition,” *Plops ONE*, vol. 10, no. 10, Oct. 2015, Art. no. e0140381.

[24] M. G. Ertegun and D. L. Rubin, “Automated grading of gliomas using deep learning in digital pathology images: A modular approach with ensemble of convolutional neural networks,” in *Proc. AMIA Annu. Symp. Proc.*, vol. 2015, Nov. 2015, pp. 1899–1908.

[25] J. S. Paul, A. J. Placard, B. A. Landman, and D. Fabbri, “Deep learning for brain tumour classification,” *Proc. SPIE, Med. Image., Biomed. Appl. Mol., Struct., Functor. Image.*, vol. 10137, Mar. 2017, Art. no. 1013710. Doi: 10.1117/12.2254195.